Spectroscopic properties of Er^{3+} ions in transparent oxyfluoride glass ceramics containing CaF_2 nano-crystals

2005 J. Phys.: Condens. Matter 17 6545

(http://iopscience.iop.org/0953-8984/17/41/024)

INSTITUTE OF PHYSICS PUBLISHING JOURNAL OF PHYSICS: CONDENSED MATTER

J. Phys.: Condens. Matter **17** (2005) 6545–6557 doi:10.1088/0953-8984/17/41/024

Spectroscopic properties of Er^{3+} ions in transparent oxyfluoride glass ceramics containing CaF_2 nano-crystals

Daqin Chen, Yuansheng Wang[1], Yunlong Yu, En Ma and Zhongjian Hu

The State Key Laboratory of Structural Chemistry, Fujian Institute of Research on the Structure of Matter, Chinese Academy of Sciences, Graduate School of Chinese Academy of Sciences, Fuzhou, Fujian 350002, People's Republic of China

E-mail: yswang@fjirsm.ac.cn

Received 16 June 2005, in final form 9 August 2005
Published 30 September 2005
Online at stacks.iop.org/JPhysCM/17/6545

Abstract

In this paper, the spectroscopic properties of Er^{3+}-doped oxyfluoride glass ceramics containing CaF_2 nano-crystals are systematically investigated. X-ray diffraction (XRD) and transmission electron microscope (TEM) experiments confirmed the formation of CaF_2 nano-crystals in the glassy matrix. Based on the Judd–Ofelt theory, the intensity parameters $\Omega_{2,4,6}$, spontaneous emission probability, radiative life, radiative quantum efficiency, width of the emission line, stimulated emission cross-section and gain spectrum were evaluated, and the effect of Er^{3+} doping concentration on the spectroscopic properties of the $^4I_{13/2} \rightarrow {}^4I_{15/2}$ transition is discussed. For glass ceramics, intense red and weak green up-conversion luminescence were observed and ascribed to two-photon absorption processes.

1. Introduction

Nowadays, Er^{3+}-doped optical materials have attracted great interest due to their possible application as media for the up-conversion laser, waveguide laser, and Er^{3+}-doped fibre amplifier (EDFA), which is one of the key elements used in the wavelength division multiplexing (WDM) network system for optical communication [1]. Due to the abundant energy transfer routes between Er^{3+} ions, efficient energy transfer can easily occur as long as the Er^{3+} are doped in a suitable host, resulting in the original luminescence. Among the numerous host materials, transparent oxyfluoride glass ceramics have attracted much attention recently because they not only have comparatively low phonon energies ascribed to fluorides, but also high chemical and mechanical stability related to oxides [2–5].

[1] Author to whom any correspondence should be addressed.

0953-8984/05/416545+13$30.00

On the other hand, among fluorides, the CaF_2 crystal is an important optical material with high solubility of both sensitizer and activator rare earth ions, and is highly transparent from 0.13 to 9.5 μm [6]. So far extensive studies have been carried out on the optical properties of rare-earth-ion-doped CaF_2 single crystals, thin films and so on [7–9]. In this paper, we have successfully prepared Er^{3+}-doped transparent glass ceramics containing CaF_2 nano-crystals, and measured their absorption spectra, emission spectra and luminescence lifetimes. Based on Judd–Ofelt theory [10, 11], the effect of Er^{3+} doping concentration on the $^4I_{13/2} \rightarrow {}^4I_{15/2}$ transition, especially the width of the emission line, the stimulated emission cross-section and the radiative quantum efficiency, were investigated. In addition, the influence of heat treatment on up-conversion emissions and the possible mechanisms of intense red up-conversion originating from the $^2F_{9/2}$ level of Er^{3+} were also discussed.

2. Experimental details

The precursor glasses were prepared with the following composition (in mol%): $45SiO_2$–$25Al_2O_3$–5CaO–10NaF–$15CaF_2$–$x$$ErF_3$ (x = 0.1, 0.5, 1.0 and 2.0), denoted as 0.1ErG, 0.5ErG, 1.0ErG and 2.0ErG respectively. For each batch, about 20 g of starting materials were fully mixed and melted in a covered platinum crucible in air atmosphere at 1350 °C for 1.5 h, and then cast into a brass mould followed by annealing at 100 °C below the glass transition temperature determined by differential thermal analysis (DTA) to relinquish the inner stress. The precursor glasses were then heated and held for 2 h at 650 °C to induce crystallization and form transparent glass ceramics (denoted as 0.1ErGC, 0.5ErGC, 1.0ErGC and 2.0ErGC respectively). In addition, the 1.0ErG sample was heated and held for 2 h at 600, 630 and 650 °C respectively (denoted as 1.0ErGCA, 1.0ErGCB and 1.0ErGCC) to investigate the effect of temperature on up-conversion emissions. To identify the crystallization phase, XRD analysis was carried out with a powder diffractometer (Rigaku DMAX2500) using Cu Kα radiation at 40 kV and 100 mA. A TEM (JEM-2010) was used to observe the microstructures of the samples. Densities were measured according to the Archimedes' principle using distilled water as medium. Refractive indices were measured by the prism minimum deviation method. The absorption spectra were recorded on a spectrophotometer (Lambda900, Perkin-Elmer) with a spectral range from 200 to 2000 nm and a resolution of 2.0 nm. The emission spectra were measured with 980 nm excitation light from a 450 W xenon lamp. By using an InP/InGaAs photomultiplier tube (PMT) detector (R5509), the infrared luminescence signals through the emission monochromator (M300) were detected. The fluorescence decay curves at 1530 nm were recorded with an NIR PMT (R5509) when excited at 980 nm by a microsecond flash lamp (μF 900). The visible up-conversion luminescence excited with a 30 mW diode laser at 980 nm was detected with a PMT detector (R928). All the measurements were carried out at room temperature.

3. Results and analysis

3.1. XRD and TEM characterizations

The typical XRD patterns obtained from precursor glass and glass ceramics with different Er^{3+} doping are shown in figure 1. The precursor glass is completely amorphous with no crystalline diffraction peaks. After crystallization, several CaF_2 crystalline peaks appear. For 2 mol% Er^{3+}-doped glass ceramic, TEM observation, as presented in figure 2, demonstrates the homogeneous distribution of spherical CaF_2 crystals with 12–16 nm in size among the glassy matrix, which is a key factor determining the optical properties of glass ceramics [12].

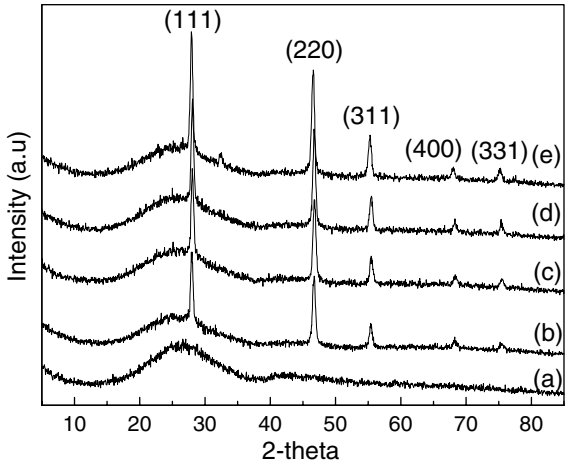

Figure 1. XRD patterns of (a) precursor glass and glass ceramic doped with (b) 0.1 mol%, (c) 0.5 mol%, (d) 1.0 mol% and (e) 2.0 mol% Er^{3+}.

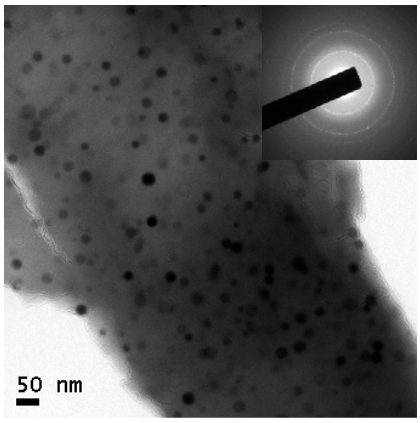

Figure 2. TEM image and the corresponding selected area electron diffraction (SAED) pattern of 2 mol% Er^{3+}-doped glass ceramic.

3.2. Absorption spectra analysis

The absorption spectra of Er^{3+} ions in precursor glasses and glass ceramics were recorded with sample thickness of 3.0 mm. As an example, the absorption spectra of 2 mol% Er^{3+}-doped precursor glass and glass ceramic in the range from 350 to 1700 are shown in figure 3. The absorption peaks, corresponding to the transitions from the ground state $^4I_{15/2}$ to the excited states, are marked in the figure. Due to the strong absorption of the host matrix in the ultraviolet range, the absorption bands at wavelength shorter than 350 nm could not be distinguished. Compared with the precursor glass, the obvious decrease of optical density for the transitions of $^4I_{15/2} \rightarrow {}^4G_{11/2}$ and $^4I_{15/2} \rightarrow {}^2H_{11/2}$ in glass ceramic implies that the circumstance of the ligand field around Er^{3+} ions must have been altered, since $^4I_{15/2} \rightarrow {}^4G_{11/2}$ and $^4I_{15/2} \rightarrow {}^2H_{11/2}$ transitions are sensitive to the environment around the active ions [13].

The analysis of spectroscopic data is required to estimate key laser parameters. Such parameters can be determined by the method based on the Judd–Ofelt theory that has been

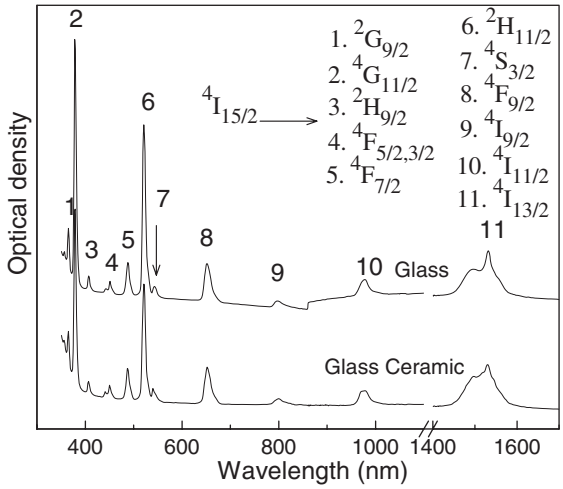

Figure 3. Room temperature absorption spectra of 2 mol% Er^{3+}-doped precursor glass and glass ceramic.

successfully applied to calculate 4f transition intensities of rare earth ions in various host materials. Its application requires the computation of three intensity parameters $\Omega_{2,4,6}$ by a fit to a number of experimental data usually obtained by ground state absorption. Thus the JO intensity parameters can be used to calculate oscillator strength of any radiative transitions, intra-shell radiative transition probabilities, radiative lifetimes as well as fluorescence branching ratios, which are useful data to access the cross-section from the emission spectra, and furthermore determine the efficiency of the material as laser and amplifier.

The experimental oscillator strength f_{exp} can be obtained from the room temperature absorption spectra by the following relation [14]:

$$f_{\mathrm{exp}} = \frac{mc^2}{\pi\lambda_{\mathrm{p}}^2 e^2}\int \sigma_{\mathrm{abs}}(\lambda)\,\mathrm{d}\lambda \tag{1}$$

where λ_{p} is the peak wavelength of the absorption band, m the mass of the electron, c the velocity of light, e the charge of the electron, and $\sigma_{\mathrm{abs}}(\lambda)$ the absorption cross-section at wavelength λ, which is defined as

$$\int \sigma_{\mathrm{abs}}(\lambda)\,\mathrm{d}\lambda = \frac{\int \mathrm{OD}(\lambda)\,\mathrm{d}\lambda}{0.43LN_0} \tag{2}$$

where N_0 is the Er^{3+} ion concentration, OD(λ) the measured optical density as a function of wavelength λ, and L the thickness of samples. The values of f_{exp} extracted from the absorption spectra of glasses and glass ceramics with different Er^{3+} concentration are listed in table 1.

The electric-dipole transition oscillator strength f_{ed} of Er^{3+} ions can be obtained from f_{exp} by

$$f_{\mathrm{ed}} = f_{\mathrm{exp}} - f_{\mathrm{md}} \tag{3}$$

where f_{md} is the oscillator strength of magnetic-dipole transition from the ground state J level to the excited state J' level and is defined as [15]

$$f_{\mathrm{md}}(J \to J') = \frac{hn}{6mc(2J+1)\lambda}|\langle 4\mathrm{f}^n[\alpha SL]J\|L+2S\|4\mathrm{f}^n[\alpha' S'L']J'\rangle|^2 \tag{4}$$

Table 1. The experimental and calculated oscillator strengths (in units of 10^{-8}) of Er^{3+} (for all concentrations of 0.1, 0.5, 1.0 and 2.0 mol%) in precursor glasses and glass ceramics; the root-mean-square (rms) errors are also presented.

	0.1ErG		0.5ErG		1.0ErG		2.0ErG		0.1ErGC		0.5ErGC		1.0ErGC		2.0ErGC	
Energy level	f_{exp}	f_{cal}	f_{exp}	f_{cal}	f_{exp}	f_{cal}	f_{exp}	f_{cal}	f_{exp}	f_{cal}	f_{exp}	f_{cal}	f_{exp}	f_{cal}	f_{exp}	f_{cal}
$^4I_{13/2}$	150.34	149.38	143.03	143.81	162.47	161.26	178.44	172.36	158.91	155.88	174.61	172.30	163.54	160.89	178.4	172.73
$^4I_{11/2}$	59.60	50.52	47.97	46.96	52.66	53.63	50.96	58.64	59.91	50.64	54.60	57.54	52.58	51.31	53.56	56.48
$^4I_{9/2}$	18.13	28.75	18.22	28.31	26.60	33.35	30.14	32.82	19.75	25.39	21.74	30.20	22.12	26.10	28.71	28.43
$^4F_{9/2}$	177.92	169.94	169.33	164.97	199.31	195.23	205.8	201.16	171.13	164.00	198.47	192.51	175.12	170.79	191.14	187.05
$^4S_{3/2}$	20.57	37.44	24.69	35.40	27.85	42.25	25.05	47.14	19.48	41.93	26.75	48.28	27.31	44.47	25.81	49.07
$^2H_{11/2}$	767.13	749.75	661.44	674.33	673.9	688.92	694.10	696.01	579.44	540.88	589.29	589.96	438.23	457.11	488.03	496.8
$^4F_{7/2}$	137.47	156.20	148.10	149.28	166.49	177.55	157.71	192.00	136.43	165.37	169.07	191.75	155.53	174.23	157.3	191.71
$^2G^4F^2H_{9/2}$	30.83	56.79	50.76	53.94	59.12	64.29	60.44	70.79	28.06	61.94	90.45	71.53	47.86	65.51	54.17	72.20
$^4G_{11/2}$	1310.10	1329.55	1209.48	1195.61	1236.93	1221.13	1235.76	1233.70	916.39	958.68	1046.04	1045.48	829.74	809.79	889.06	880.09
Rms error (%)	3.07		1.75		2.07		3.00		6.88		3.06		4.26		4.48	

Table 2. Ω_t parameters of Er^{3+} in the different samples.

Sample	Ω_2 (10^{-20} cm^2)	Ω_4 (10^{-20} cm^2)	Ω_6 (10^{-20} cm^2)
0.1ErG	5.015	1.382	0.995
0.1ErGC	3.484	1.221	1.123
0.5ErG	4.435	1.363	0.941
0.5ErGC	3.720	1.455	1.293
1.0ErG	4.387	1.605	1.123
1.0ErGCA	3.307	1.316	1.056
1.0ErGCB	3.215	1.296	1.154
1.0ErGCC	2.785	1.253	1.191
2.0ErG	4.446	1.571	1.253
2.0ErGC	3.023	1.364	1.314

where $\langle 4f^n[\alpha SL]J\|L+2S\|4f^n[\alpha' S'L']J'\rangle$ is the reduced matrix element for the operator $L+2S$ and can be calculated from the formula proposed by Weber [15], h is the Planck constant, n is the refractive index of samples and is assumed to be the same at different wavelengths ($n = 1.520$) for precursor glasses and glass ceramics and $2J + 1$ is the degeneracy of the ground state of Er^{3+}. The magnetic-dipole transitions are parity allowed between states of f^{11} (Er^{3+}) configuration and subject to selection rules $\Delta S = \Delta L = 0, \Delta J = 0, \pm 1$ ($0 \leftrightarrow 0$ forbidden) in the Russel–Saunders limit.

Based on the Judd–Ofelt theory [10, 11], the electric-dipole transition oscillator strength f_{ed} is expressed as

$$f_{ed}(J \to J') = \frac{8\pi^2 mc}{3h(2J+1)\lambda_p}\frac{(n^2+2)^2}{9n}\sum_{t=2,4,6}\Omega_t|\langle {}^4I_{15/2}\|U^{(t)}\|4f^n[\alpha' S'L']J'\rangle|^2 \tag{5}$$

where $U^{(t)}$ ($t = 2, 4, 6$) are unit tensor operators and their matrix elements had been calculated by Carnall *et al* [16]. By a least-root-mean-square fitting between equations (3) and (5) the three intensity parameters Ω_2, Ω_4 and Ω_6 were obtained and listed in table 2. From the intensity parameters, the electric-dipole transition oscillator strengths were obtained from equation (5), and then the theoretical oscillator strength was calculated by

$$f_{cal} = f_{ed} + f_{md} \tag{6}$$

and is listed in table 1.

In the application of the standard Judd–Ofelt approach, the intensity parameters are just derived from the absorption spectra and their values indicate the variation of the Er^{3+} environment from glass to glass ceramics. The values for glass ceramics should be attributed to the total contribution of Er^{3+} in glass matrix and nano-crystals. According to Judd–Ofelt theory, Ω_2 is sensitive to the environmental configuration symmetry of rare earth ions, and it decreases with the host changing from oxides to fluorides [17–20]. On the other hand, Ω_6 usually increases with decreasing covalence between rare earth ions and the surrounding elements [21]. From precursor glasses to glass ceramics doped with different Er^{3+} concentrations, the decrease of Ω_2 and the increase of Ω_6 suggest that Er^{3+} had been incorporated into CaF_2 nano-crystals after crystallization.

3.3. Spectroscopic properties

3.3.1. The $^4I_{13/2} \to {}^4I_{15/2}$ transition. Firstly, this work was focused on the $^4I_{13/2} \to {}^4I_{15/2}$ transition of Er^{3+}. Once the intensity parameters are derived, the spontaneous emission probabilities of the electric-dipole transition A_{ed} and the magnetic-dipole transition

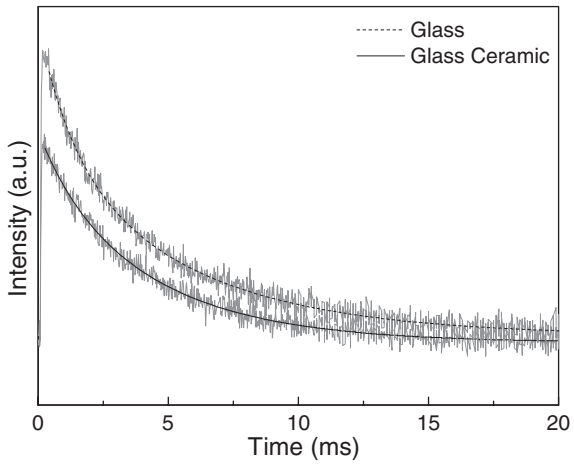

Figure 4. Room temperature fluorescence decay curves of Er^{3+} in 2 mol% Er^{3+}-doped precursor glass and glass ceramic recorded at 1530 nm. The fitted results of single-exponential decay are 4.35 and 5.48 ms, respectively.

A_{md}, corresponding to the $^4I_{13/2} \rightarrow {}^4I_{15/2}$ transition, can be calculated by the following relations [22]:

$$A_{\mathrm{ed}}(13/2 \rightarrow 15/2) = \frac{64\pi^4 e^2}{3h(2J+1)\lambda_{\mathrm{e}}^3} \frac{n(n^2+2)^2}{9} \sum_{t=2,4,6} \Omega_t |\langle {}^4I_{13/2} \| U^{(t)} \| {}^4I_{15/2} \rangle|^2 \tag{7}$$

$$A_{\mathrm{md}}(13/2 \rightarrow 15/2) = \frac{4\pi^2 e^2 h n^3}{3m^2 c^2 (2J+1)\lambda_{\mathrm{e}}^3} |\langle {}^4I_{13/2} \| L + 2S \| {}^4I_{15/2} \rangle|^2 \tag{8}$$

where λ_{e} is emission peak wavelength. Then the total spontaneous emission probability A_{total} is

$$A_{\mathrm{total}} = A_{\mathrm{ed}} + A_{\mathrm{md}}. \tag{9}$$

The radiative lifetime is

$$t_{\mathrm{r}} = 1/A_{\mathrm{total}} \tag{10}$$

and the radiative quantum efficiency is defined as

$$\eta = t_{\mathrm{m}}/t_{\mathrm{r}} = t_{\mathrm{m}} \cdot A_{\mathrm{total}} \tag{11}$$

where t_{m} is the luminescence lifetime obtainable from the fluorescence decay curve. As an example, the decay curves of 2 mol% Er^{3+}-doped precursor glass and glass ceramic are shown in figure 4. By fitting the decay curve the lifetime of $^4I_{13/2}$ level could be estimated. The values of A_{ed}, A_{md}, A_{total}, t_{r}, t_{m}, and η for precursor glass and glass ceramics doped with different Er^{3+} concentrations are listed in table 3.

The emission spectra of the $^4I_{13/2} \rightarrow {}^4I_{15/2}$ transition for precursor glasses and glass ceramics doped with different Er^{3+} concentrations are presented in figures 5 and 6, from which the emission peak wavelength λ_{e} was obtained, and the width of the emission band $\Delta\lambda_{\mathrm{eff}}$ was calculated by

$$\Delta\lambda_{\mathrm{eff}} = \frac{\int I(\lambda)\,\mathrm{d}\lambda}{I_{\mathrm{max}}} \tag{12}$$

where $I(\lambda)$ is the emission intensity at wavelength λ, and I_{max} the emission intensity at peak emission wavelength. The stimulated emission cross-section of the $^4I_{13/2} \rightarrow {}^4I_{15/2}$ transition

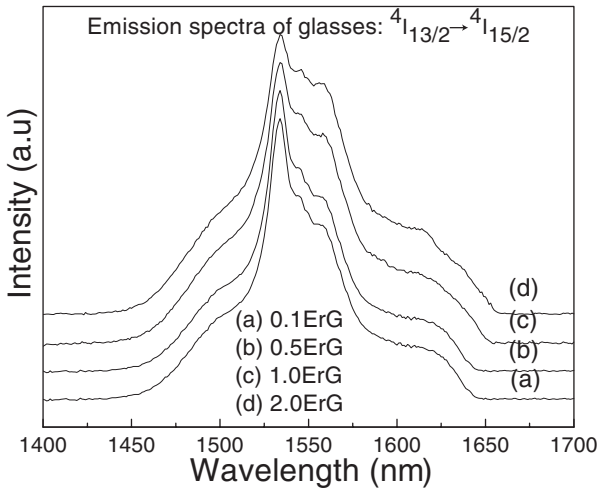

Figure 5. Room temperature emission spectra of Er^{3+} in the precursor glasses.

Table 3. Some spectroscopic parameters corresponding to the $^4I_{13/2} \rightarrow {}^4I_{15/2}$ transition of Er^{3+}.

Sample	A_{ed} (s^{-1})	A_{md} (s^{-1})	A_{total} (s^{-1})	t_r (ms)	t_m (ms)	η (%)	λ_e (nm)	$\Delta\lambda_{eff}$ (nm)	σ_{em} (λ_e) (10^{-20} cm^2)
0.1ErG	75.21	35.69	110.90	9.02	7.93	88	1534	61	0.58
0.5ErG	71.51	35.63	107.14	9.33	7.23	83	1534	67	0.51
1.0ErG	84.45	35.71	120.16	8.32	6.05	73	1534	73	0.53
2.0ErG	92.69	35.74	128.43	7.79	4.35	56	1534	82	0.50
0.1ErGC	80.69	35.52	116.21	8.61	8.35	97	1534	60	0.62
0.5ErGC	93.01	35.37	128.38	7.79	7.56	97	1532	70	0.58
1.0ErGC	84.67	35.21	119.88	8.34	6.57	79	1533	81	0.47
2.0ErGC	91.35	34.70	126.05	7.93	5.48	69	1546	91	0.46

could be estimated from emission spectra with the help of the Fuchtbauer–Landenburg equation [23]

$$\sigma_{em}(\lambda) = \frac{\lambda^5 \beta I(\lambda)}{8\pi c n^2 \int \lambda I(\lambda)\, d\lambda} A_{total} \tag{13}$$

where $I(\lambda)/\int \lambda I(\lambda)\, d\lambda$ is the normalized line-shape function of the experimental emission spectrum $I(\lambda)$, and β the branching ratio of the $^4I_{13/2} \rightarrow {}^4I_{15/2}$ transition which equals unity in this case since this transition is the unique radiative decay channel for $^4I_{13/2}$ state. The value of λ_e, $\Delta\lambda_{eff}$, and $\sigma_{em}(\lambda_e)$ for precursor glasses and glass ceramics doped with different Er^{3+} concentrations are also listed in table 3.

Once the absorption and emission cross-section spectra have been derived, the gain cross-section spectrum $g(\lambda)$ can be computed using following equation:

$$g(\lambda) = P\sigma_{em}(\lambda) - (1 - P)\sigma_{abs}(\lambda) \tag{14}$$

where the population inversion P is the ratio of Er^{3+} concentration in the lasing state $^4I_{13/2}$ to that in the ground state. As an example, figure 7 displays the gain spectra for 1.0 mol% Er^{3+}-doped glass ceramic as a function of the population inversion P. Obviously, the gain

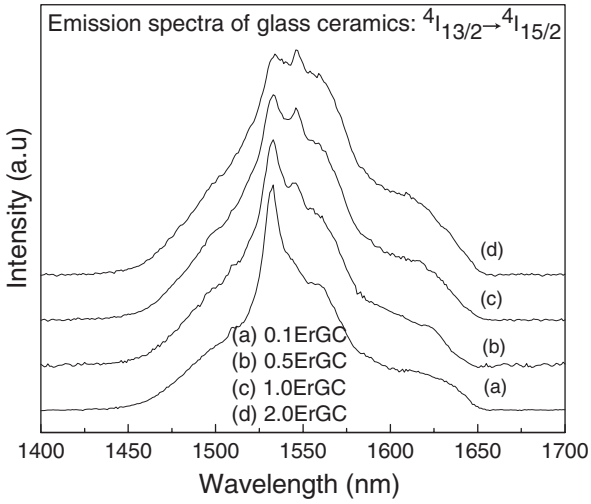

Figure 6. Room temperature emission spectra of Er^{3+} in the glass ceramics.

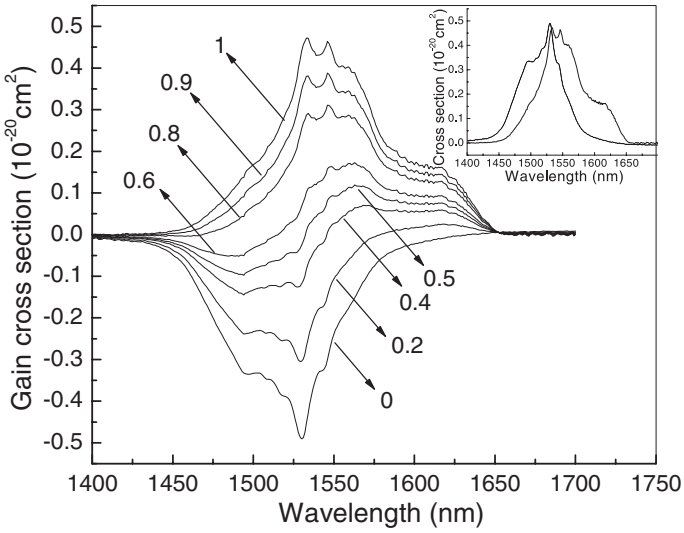

Figure 7. Gain cross-section spectra of the $^4I_{13/2} \rightarrow {}^4I_{15/2}$ transition of Er^{3+} in 1.0ErGC. The respective population inversion P is indicated. The inset shows the absorption (dotted line) and stimulated emission (solid line) cross-sections corresponding to the $^4I_{13/2} \rightarrow {}^4I_{15/2}$ transition, respectively.

spectra in the range from 1530 to 1565 nm are relatively flat for the population inversion from 0.8 to 1.0.

3.3.2. Up-conversion luminescence. By exciting at 980 nm with a diode laser, up-conversion emission of Er^{3+} at about 550 (green luminescence) and 660 nm (red luminescence) were recorded for glass ceramics. Figure 8 shows the up-conversion luminescence spectra in 1.0 mol % Er^{3+}-doped precursor glass and glass ceramics. The up-conversion luminescence can hardly be observed in the precursor glass, while it is strong in the glass ceramics. The emission

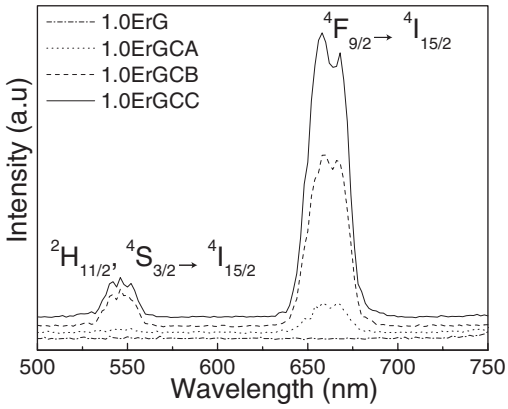

Figure 8. Visible up-conversion emission spectra in 1.0 mol% Er^{3+}-doped precursor glass and glass ceramics obtained by heating at different temperatures.

Table 4. Comparison of the spectroscopic parameters of Er^{3+} in different host materials.

Host materials	λ_e (nm)	$\Delta\lambda_{eff}$ (nm)	σ_e (10^{-20} cm^2)	η (%)	Reference
0.1ErGC	1534	60	0.62	97	This work
1.0ErGC	1533	81	0.47	79	This work
ZBLAN	1550	82	0.42	91	[28]
ED-2 (silicate)	—	40	0.65	100	[29]
LGS-E7 (phosphate)	1545	46	0.86	86	[29]
$45Bi_2O_3$–$55B_2O_3$	1523	81	0.71	23	[26]

bands are assigned to $^2H_{11/2}$, $^4S_{3/2} \rightarrow {}^4I_{15/2}$ and $^4F_{9/2} \rightarrow {}^4I_{15/2}$ transitions, respectively. The intensity of red luminescence is stronger than that of green, and both of them increase with increasing heat treatment temperature of the sample.

4. Discussion

In order to satisfy the need for the increment of information capacity and improve the performance of the WDM network, a medium with a width and flat gain at about 1530 nm, which is related to the width of the emission band $\Delta\lambda_{eff}$, is required for the EDFA. As shown in table 3, for precursor glasses, the $\Delta\lambda_{eff}$ increases with the increasing of Er^{3+} concentration. This suggests that the local environment tends to be disordered with the increasing of Er^{3+} doping level, resulting in the broadening of the Er^{3+} emission band at about 1530 nm [24–26]. For glass ceramics, the $\Delta\lambda_{eff}$ values are slightly larger than those of precursor glasses. These may partly be attributed to the lower structural symmetry of the host due to the incorporation of Er^{3+} into CaF_2 [27]. As a result, the Stark splitting of Er^{3+} level increases, which leads to a larger $\Delta\lambda_{eff}$ value. In addition, the complementary emissions of Er^{3+} in CaF_2 and the residual Er^{3+} in glass matrix may also contribute to them. At present, the silica-based and ZBLAN glasses are widely used as the media of the EDFA. As listed in table 4, the $\Delta\lambda_{eff}$ values of the silica-based and ZBLAN glasses are about 40 and 80 nm, respectively. It is evident that Er^{3+}-doped glasses and glass ceramics have an emission band wider than that of the silica-based glass and comparable to that of the ZBLAN glass.

A large stimulated emission cross-section and high radiative quantum efficiency benefit the high gain and low threshold in laser operation. As shown in table 3, the value of the

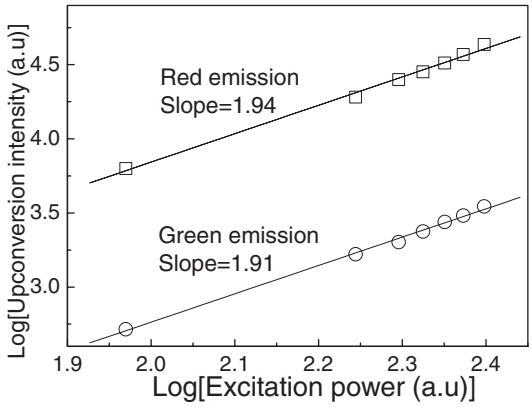

Figure 9. Log–log plots of the green and red emission intensities as a function of the excitation power at 980 nm for 1.0 mol% Er^{3+}-doped glass ceramic.

stimulated cross-section σ_e varies with the Er^{3+} doping concentration for precursor glasses and glass ceramics. The maximum emission cross-section is obtained for glass ceramic doped with 0.1 mol% Er^{3+}. For precursor glasses and glass ceramics, the radiative quantum efficiency decreases with increasing of Er^{3+} doping level due to the enhancing of energy transfer probability between Er^{3+} ions. Moreover, the quantum efficiencies of the glass ceramics are obviously higher than that of the precursor glasses, probably due to the incorporation of Er^{3+} into CaF_2 with lower phonon energy that decreases non-radiative relaxation. For glass ceramics doped with 0.1 and 0.5 mol% Er^{3+}, the quantum efficiencies reach 97%. As a comparison, the stimulated emission cross-section and the radiative quantum efficiency of Er^{3+} in the investigated glass ceramics and other hosts are listed in table 4.

In up-conversion processes the emission intensity I_{UP} is proportional to a power n of the IR excitation intensity I_{IR}, i.e.

$$I_{UP} \propto (I_{IR})^n \tag{15}$$

where n is the number of IR photons absorbed to populate per visible photon emitting. A plot of the logarithm of I_{UP} versus the logarithm of I_{IR} should yield a straight line with slope n. Such a plot for red and green up-conversion emissions in 1.0 mol% Er^{3+}-doped glass ceramic is shown in figure 9, and the values of n obtained are 1.94 and 1.91, respectively, indicating that both red and green emissions from $^2H_{11/2}$, $^3S_{3/2}$ and $^4F_{9/2}$ levels are attributed to the two-photon up-conversion process.

Based on the quadratic dependence of excitation power and the energy matching conditions, the possible up-conversion mechanisms are presented in the simplified energy level diagram of Er^{3+} in figure 10. Two possible mechanisms for green emission could be described as (a) excited energy absorption (ESA), and (b) energy transfer up-conversion (ETU) [30]. In these two mechanisms, the electrons on the $^4I_{11/2}$ level are excited to the $^4F_{7/2}$ level, and then $^4S_{3/2}$ and $^4H_{11/2}$ levels are populated by multi-phonon relaxation from $^4F_{7/2}$ level. After crystallization, Er^{3+} are incorporated into nano-crystals in glass ceramics and then the ions are located closer to each other than those uniformly dispersed in the precursor glasses. The short distances between Er^{3+} ions in CaF_2 nano-crystals favour interionic interactions, resulting in an efficient near resonant cross relaxation process (CR) involving erbium–erbium pairs ($^4F_{7/2}$, $^4I_{15/2} \rightarrow {}^4F_{9/2}$, $^4I_{13/2}$). In this case, the $^4F_{9/2}$ level is greatly populated from the $^4F_{7/2}$ level by cross relaxation, which induces intense red emission. Another way to augment the population of $^4F_{9/2}$ may be based on the following processes: $^4I_{13/2}$+ a photon $\rightarrow$ $^4F_{9/2}$ (ESA), and

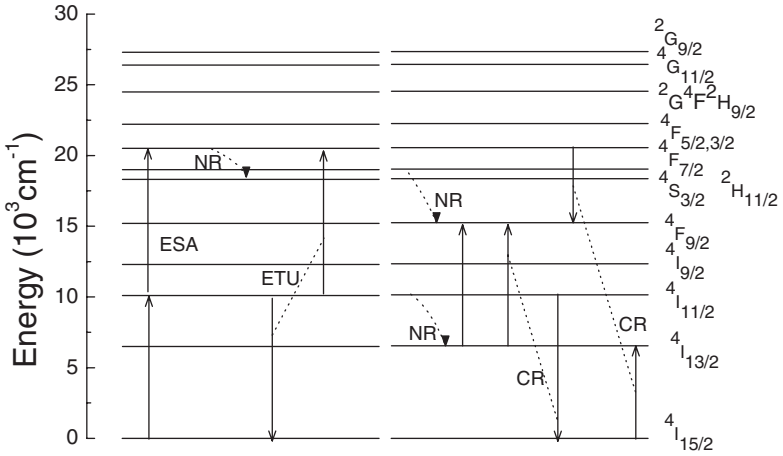

Figure 10. Simplified energy level diagram for Er^{3+} in glass ceramics and the possible up-conversion mechanisms.

$^4I_{13/2} + {}^4I_{11/2} \rightarrow {}^4I_{15/2} + {}^4F_{9/2}$ (CR). The $^4I_{13/2}$ level is populated owing to the non-radiative relaxation from the upper $^4I_{11/2}$ level. Besides, the non-radiative relaxation from $^4S_{3/2}$ to $^4F_{9/2}$ also contributes to the red emission. With increasing of heat treatment temperature, the emission intensity is intensified. This could be ascribed to more Er^{3+} ions incorporated into CaF_2 crystals, verified by the changes of the intensity parameters $\Omega_{2,4,6}$ versus heating temperature, i.e., the Ω_2 and Ω_4 values decrease significantly and Ω_6 increases slightly with increasing of the temperature.

5. Conclusions

The absorption, emission spectra and luminescence lifetimes of Er^{3+}-doped transparent glass ceramics containing CaF_2 nano-crystals were measured. Based on the Judd–Ofelt theory, the intensity parameters and the spectroscopic parameters related to the laser performance were evaluated from the experimental data. The effect of Er^{3+} concentration on spectroscopic properties of the $^4I_{13/2} \rightarrow {}^4I_{15/2}$ transition, including the width of the emission line, the stimulated emission cross-section and the radiative quantum efficiency, were investigated. The maximum width of the emission line was about 91 nm for 2.0 mol% Er^{3+}-doped glass ceramic. The maximum radiative quantum efficiency and stimulated emission cross-section of 97% and 0.62×10^{-20} cm^2 respectively were achieved in 0.1 mol% Er^{3+}-doped glass ceramic.

Visible up-conversion emissions were also studied for 1.0 mol% Er^{3+}-doped sample. Intense red and weak green up-conversion emissions were observed for glass ceramics, and both intensities increased with increasing of the heat treatment temperature, probably due to the change of ligand field surrounding Er^{3+} ions caused by the incorporation of Er^{3+} into precipitated CaF_2 nano-crystals with lower phonon energy. The quadratic pump power dependence of the up-conversion luminescence intensity for red and green emissions indicates that the transitions for both up-conversion emissions were ascribed to the two-photon absorption process.

Acknowledgments

This work was supported by grants from the Natural Science Foundation of Fujian Province China (project No A0320001), the Ministry of Science and Technology of China (project No

2003BA323C) and the State Key Laboratory of Structural Chemistry of China (project No. 050005).

References

[1] Becker P C, Olsson N A and Simpson J R 1999 *Erbium Doped Fiber Amplifiers: Fundamentals and Technology* (San Diego, CA: Academic)
[2] Wang Y and Ohwaki J 1993 *Appl. Phys. Lett.* **63** 3268
[3] Dejneka M J 1998 *J. Non-Cryst. Solids* **239** 149
[4] Fu J, Parker J M, Flower P S and Brown R M 2002 *MRS Bull.* **37** 1843
[5] Lahoz F, Martin I R and Mendez-Ramos J 2004 *J. Chem. Phys.* **120** 6180
[6] Lucca A, Jacquemet M, Druon F, Balembois F, Georges P, Camy P, Doualan J L and Moncorgé R 2004 *Opt. Lett.* **29** 1879
[7] Jon-Paul R W and Roger J R 2004 *J. Lumin.* **66/67** 219
[8] Falin M L, Gerasimov K I, Latypov V A, Leushin A M, Bill H and Lovy D 2004 *J. Lumin.* **102/103** 239
[9] Balaji T, Lifante G, Daran E, Legros R and Lacoste G 1999 *Thin Solid Films* **339** 187
[10] Judd B R 1962 *Phys. Rev.* **127** 750
[11] Ofelt G S 1962 *J. Chem. Phys.* **37** 511
[12] Tick P A 1998 *Opt. Lett.* **23** 1904
[13] Jorgensen C K and Judd B R 1964 *Mol. Phys.* **8** 281
[14] Weber W J, Matsinger B H, Donan V L and Surratt G T 1972 *J. Chem. Phys.* **57** 562
[15] Weber M J 1967 *Phys. Rev.* **157** 262
[16] Carnal W T, Fields P R and Rajnak K 1968 *J. Chem. Phys.* **49** 4424
[17] Zou X and Izumitani T 1993 *J. Non-Cryst. Solids* **162** 68
[18] Bettinelli M, Speghini A, Ferrari M and Montagna M 1996 *J. Non-Cryst. Solids* **201** 211
[19] Oomen E W J L and van Dongen A M A 1989 *J. Non-Cryst. Solids* **111** 205
[20] Nageno Y, Takebe H, Morinaga K and Izumitani T 1994 *J. Non-Cryst. Solids* **169** 288
[21] Tanabe S, Ohyagi T, Soga N and Hanada T 1992 *Phys. Rev.* B **46** 3305
[22] Ivanova T Y, Man'shina A A, Kurochkin A V, Tver'yanovich Y S and Smirnov V B 2002 *J. Non-Cryst. Solids* **298** 7
[23] Kaminskii A A 1989 *Laser Crystals: Their Physics and Properties* (New York: Springer)
[24] Kim M J, Mebratu G K, Sung J Y and Shin J H 2003 *J. Non-Cryst. Solids* **315** 312
[25] El-Mallawany R, Patra A, Friend C S, Kapoor R and Prasad P N 2004 *Opt. Mater.* **26** 267
[26] Chen Y, Huang Y, Huang M, Chen R and Luo Z 2004 *Opt. Mater.* **25** 271
[27] Kumar G A, Riman R, Chae S C, Jang Y N, Bae I K and Moon H S 2004 *J. Appl. Phys.* **95** 3243
[28] Wetenkamp L, West G F and Tobben H 1992 *J. Non-Cryst. Solids* **140** 35
[29] Gapontsev V P, Matitsin S M, Isineev A A and Kravchenko V B 1982 *Opt. Laser Technol.* **14** 189
[30] Vander Ziel J P, Van Uitert L G, Grodkiewicz W H and Mikulgak R M 1986 *J. Appl. Phys.* **60** 4262